

Design and verification of q-axis perturbation based active islanding detection schemes for DG systems

Praveen Raj Rajaswamy Sarojam¹, Joseph Sarojini Savier²

¹Department of Electrical and Electronics Engineering, Mar Baselios College of Engineering and Technology, Kerala, India

²Department of Electrical and Electronics Engineering, College of Engineering, Kerala, India

Article Info

Article history:

Received Aug 4, 2023

Revised Oct 28, 2023

Accepted Nov 16, 2023

Keywords:

Even harmonic perturbation
Grid synchronized distributed generation
Islanding detection methods
Rate of change of frequency
Sub-harmonic perturbation
Complementary reactive power perturbation

ABSTRACT

The penetration of grid integrated distributed generation (DG) in the present decade, has benefited rural communities, the environment, and the power sector. These renewable power sources based DGs could eliminate the need of extensive transmission networks, especially in remote areas, reduce emissions and improve power supply reliability. A significant drawback of grid integrated DG systems is the islanding of DG units, which puts workers' safety at risk and raises the possibility of damaging electrical infrastructure. Therefore, islanding detection techniques are used to reduce the danger associated with islanded functioning of DG units. Fast detection, small non detection area and less power quality disturbance are the major requirements of any islanding detection method. To address this issue of islanding, researchers have proposed various islanding detection strategies. This paper compares various q-axis controller-based islanding identification approaches: sub-harmonic perturbation (SHP), complementary reactive power perturbation (CRPP), and even harmonic perturbation (EHP). In all three proposed methodologies, the perturbations introduced result in frequency deviations surpassing the predefined threshold values. But the time of islanding detection is least in the CRPP approach. CRPP can also drift the total harmonic distortion (THD) beyond the corresponding threshold in an appreciable way. The performance of these (Islanding detection methods) IDMs is evaluated through simulations using MATLAB-Simulink on a PV fed DG. The efficacy of the comparative analysis is ensured with necessary waveforms.

This is an open access article under the [CC BY-SA](https://creativecommons.org/licenses/by-sa/4.0/) license.



Corresponding Author:

Praveen Raj Rajaswamy Sarojam
Department of Electrical and Electronics Engineering
Mar Baselios College of Engineering and Technology
Nalanchira, Kerala, India
Email: india.praveenraj@gmail.com

1. INTRODUCTION

Distributed generation (DG) is essential for powering remote areas distant from centralized power stations, like hydroelectric or thermal plants, which pose economic challenges. The continuous evolution of DGs, driven by advancements in power electronics, has further boosted their popularity [1], [2]. The significant reduction in transmission losses associated with renewable energy sources (RES)-fed DGs is an added advantage. Integrating these DGs with the grid is crucial and beneficial [3], [4]. However, before achieving synchronization, several challenges need to be resolved. One critical concern is the issue of islanding, which can lead to serious problems and even fatalities. To address this, the IEEE 1547 standard mandates that DGs must disconnect from the electrical power system (EPS) within a short 2-second timeframe if an islanding

situation occurs. According to IEEE1547 standard, islanding occurs when a DG keeps supplying power to an area despite disconnection from the bulk EPS [5]. Both voluntary and involuntary islanding states can occur in a power system.

In grid synchronized DG (GSDG), when the local load exceeds power generation, the grid shares the deficit power. Conversely, when DG produces more power than needed, the surplus is fed back to the grid. This makes GSDG operation necessary and beneficial. During loss of mains (islanding), the DG solely supplies the load. Researchers have formulated several remote as well as local islanding detection methods (IDMs). The local IDMs can further be categorized into passive, active and hybrid IDMs. The communication between utility grid and DG is employed in remote IDMs, to monitor and identify unintended islanding. This method is advantageous as it is not affected by local power balance, causes no grid disruptions, and can be customized for different grid conditions, eliminating non-detection zone (NDZ) issues. Some examples of remote IDM include impedance insertion method [6], power line signal scheme, signal produced by disconnect [7], and transfer trip scheme [8]. These IDMs theoretically have no NDZ but can be quite expensive. Passive IDM employs various electrical parameters at point of common coupling (PCC), such as voltage variation beyond thresholds [9], frequency variation beyond thresholds [10], voltage total harmonic distortion (THD) going above the desired limits, current THD going above the desired limits [11], rate of change of reactive power [12], harmonic signatures [13] in order to recognize an islanding scenario. As the grid's power sharing approaches zero, passive islanding detection methods (IDMs) encounter challenges in discerning islanding events due to the diminishing significance of deviations in PCC parameters. This limitation encouraged the development of active IDMs. Active IDMs purposefully cause the grid and local load at PCC to be perturbed by DG inverters. The low impedance of the DG absorbs these disturbances while it is synchronized with the grid. However, during islanding, these injected disturbances result in the divergence of one or more PCC parameters from their predefined thresholds, resulting in the relay tripping. High frequency signals injection techniques [14], d axis current injection [15], reactive power injection, sandia Frequency [16], are a few examples of active IDMs.

Active IDMs can have unfavorable impact on power quality (PQ) even though they yield less NDZ [17]. The integration of passive and active islanding detection methods (IDMs) gives rise to the development of Hybrid IDMs. D axis current injection combined with rate of change of frequency (ROCOF) [18], active power change as the active IDM with rate of change of voltage as passive IDM [19], Sandia frequency shift (SFS), and rate of change of frequency (ROCOF) [20] are some of the hybrid IDMs presented in the literature. Hybrid methods enable the utilization of the advantages offered by both approaches, while the limitations inherent to each method are not avoidable.

This paper mainly deals with the comparison of the q-axis perturbation-based IDMs. The d-axis disturbances are variations in the active power component of the electrical variables. They are primarily associated with changes in the real power component and are more relevant for power system control, stability, and load management. The q-axis disturbances cause variations in the electrical variables such as voltage magnitude and frequency. q-axis disturbances are highly effective in detecting islanding events, as they are less likely to occur during normal grid-connected operation. Different q axis perturbation-based islanding identification schemes are summarized in Table 1.

Table 1. Comparison of various performance parameters of Q axis perturbation-based IDMs

Ref	Non-detection zone (NDZ)	Fault detection zone (FDZ)	Identification time	Power quality (PQ)
[21]	Small NDZ	NO FDZ	0.17s	Affects PQ
[22]	Very small, but non-zero NDZ	Asymmetrical fault leads to false detection	0.433 s	Affects PQ
[23]	No NDZ	FDZ to be analyzed	0.1785s	Affects PQ
[24]	Very small	-	0.25s	Affects PQ
[25]	No NDZ	NO FDZ	0.12s	Affects PQ Slightly
[26]	No NDZ	Exists FDZ when grid frequency exceeds $\pm 0.5\text{Hz}$	0.18s	Affects PQ but within limits
[27]	No NDZ	-	0.15s	Affects PQ
[28]	NDZ exists	-	0.16s	Larger PQ issues when NDZ is reduced

An effective islanding detection scheme should satisfy the following criteria: i) Identify islanding occurrences across a diverse range of operational scenarios; ii) Discriminate between islanding and non-islanding events; iii) Quick detection time (< 2 seconds) is desirable; iv) Compatible with other existing DGs; and v) Simple and cheap in implementation. Therefore, a simple and robust islanding detection method with minimum detection time is inevitable in GSDGs. Three active methods, based on perturbations through q axis current, are presented and compared in this paper. As the reactive power is a deciding factor of frequency, the response to detect islanding state could be ROCOF.

The major contributions of this work are: i) Comparative analysis of NDZ and FDZ is performed; ii) Comparative analysis regarding THDs during grid integrated mode is carried out; iii) Comparative analysis of THDs during islanded mode is also presented; and iv) Detection time for different load quality factors (QF) = 5 is presented for the three methods. The paper is organized as: i) The three active islanding detection methods along with its response is presented in section 2; ii) Response of the passive methods presented in section 3; iii) Results and waveforms necessary for the analysis are depicted in section 4; iv) Comparison of the three approaches is depicted in section 5; and v) conclusion in section 6.

2. THE PROPOSED SCHEMES FOR ISLANDING DETECTION

In the proposed work three q axis perturbation based active islanding detection methods are presented, analyzed and are compared in various perspectives. As q axis disturbances do not pose any stability issues to the DG or utility grid, whereas the d axis perturbations can cause stability problems. The proposed system in the block schematic is presented in Figure 1.

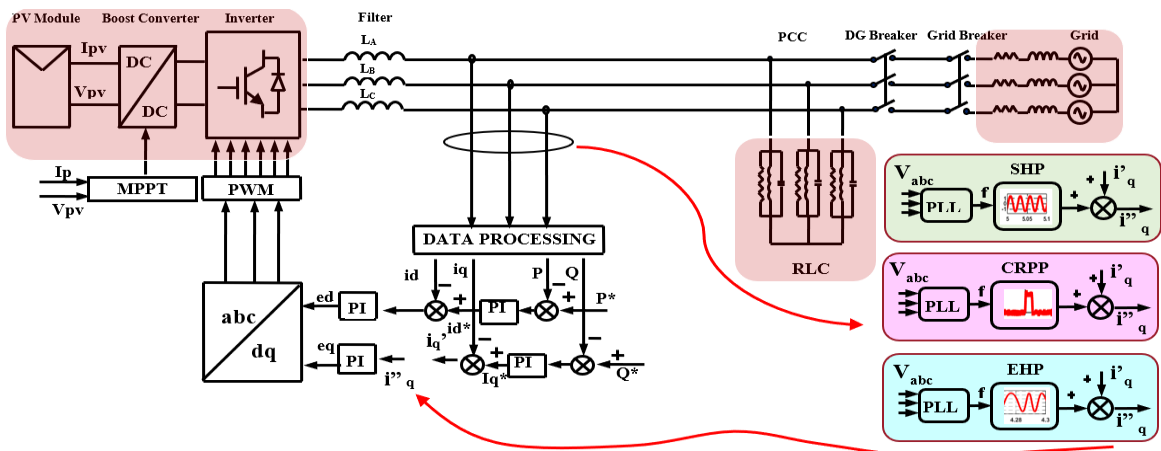


Figure 1. Block diagram of the proposed system with three q axis control methods

2.1. Active islanding detection scheme -I (Sub-harmonic perturbation (SHP))

Sub harmonic perturbation (SHP) is injected in the q axis current in the d-q frame. So, the perturbation fed into the grid at PCC is in such a level that the grid power quality (PQ) is not deteriorated beyond the threshold level. In response to the modifications in the q axis current, DG frequency signatures change. When the DG is integrated to bulk EPS, voltage at PCC, V_{pcc} is same as grid voltage, V_{grid} and is presented in (1). The frequency:

$$V_{pcc} = V_{grid} \tag{1}$$

the d axis and q axis current equations of DG inverter is given by (2),

$$\begin{bmatrix} i_d \\ i_q \end{bmatrix} = \begin{bmatrix} i_{dinv} \\ i_{qinv} \end{bmatrix} \tag{2}$$

The current equations are altered as follows when SHP is injected as in (3) and (4).

$$\begin{bmatrix} i_d \\ i_q \end{bmatrix} = \begin{bmatrix} i_{dinv} \\ i_{qinv} + i_{qpert} \end{bmatrix} \tag{3}$$

$$i_{qpert} = i_{dinv} \sin(\omega_{pert}t) \tag{4}$$

i_{dinv} is DG inverter current. After the Park's transformation, the A phase voltage is expressed as in (5).

$$V_a = Z_{zero}i_d \sin(\omega_p t) + Z_{pos}i_d \sin(\omega_p t + \phi_i) + Z_{neg}i_d \sin(\omega_p t + \phi_i) \tag{5}$$

Where:

$$\begin{aligned}\omega_p &= 2\pi f_p, p = 0,1,2 \\ f_2 &= f_0 + f_{\text{pert}} \\ f_1 &= f_0 - f_{\text{pert}} \\ \phi_i &= -\tan^{-1}\left(R\left(\omega_i C - \frac{1}{\omega_i L}\right)\right) i = 1,2 \\ Z_x &= \frac{1}{\left(\left(\frac{1}{R}\right)^2 + \left(\omega_x C - \frac{1}{\omega_x L}\right)^2\right)^{\frac{1}{2}}} \\ x &= 0,1,2\end{aligned}$$

The introduction of sub-harmonic injection in the q-axis current induces oscillations in the distributed DG frequency during an islanding state, while such oscillations are not manifested in a grid connected distributed generation (GCDG) state. When the ROCOF surpasses the designated threshold, the inverter disengages from grid energization.

2.2. Active islanding detection scheme II – (Complementary reactive power perturbation (CRPP))

In the second islanding identification approach, complementary reactive power perturbation (CRPP) is injected at PCC. These perturbations cause the frequency to move away from the threshold value during islanding scenario. However, there is no such frequency deviation during grid synchronized mode operation of DGs. The active and reactive load powers are given by (6) and (7).

$$P_{\text{Load}} = P_{\text{DG}} + \Delta P \quad (6)$$

$$Q_{\text{Load}} = Q_{\text{DG}} + \Delta Q \quad (7)$$

ΔP and ΔQ are the grid share components. The load – power components are expressed as in (8) and (9).

$$P_{\text{Load}} = 3 \frac{V_{\text{PCC}}^2}{R} \quad (8)$$

$$Q_{\text{Load}} = 3V_{\text{PCC}}^2 \left(\frac{1}{2\pi fL} - 2\pi fC\right) \quad (9)$$

The resonant frequency and load quality factors are given by (10) and (11).

$$f_r = \frac{1}{2\pi\sqrt{LC}} \quad (10)$$

$$Q = R\sqrt{\frac{C}{L}} \quad (11)$$

The frequency, f in the grid islanded mode is computed from (12).

$$f = \frac{f_r}{2} \left[\sqrt{\left(\frac{Q_{\text{Load}}}{Q_{\text{P}_{\text{Load}}}}\right)^2 + 4} - \frac{Q_{\text{Load}}}{Q_{\text{P}_{\text{Load}}}} \right] \quad (12)$$

During loss of mains, frequency f_i be computed from (13)-(16).

$$P'_{\text{Load}} = 3 \frac{V'^2_{\text{PCC}}}{R} \quad (13)$$

$$Q'_{\text{Load}} = 3V'^2_{\text{PCC}} \left(\frac{1}{2\pi fL} - 2\pi fC\right) \quad (14)$$

$$f_i = \frac{f_r}{2} \left[\sqrt{\left(\frac{Q_{\text{DG}}}{Q_{\text{P}_{\text{DG}}}}\right)^2 + 4} - \frac{Q_{\text{DG}}}{Q_{\text{P}_{\text{DG}}}} \right] \quad (15)$$

$$f_i = \frac{f}{4} \left[\sqrt{\left(\frac{Q_{\text{DG}}}{Q_{\text{P}_{\text{DG}}}}\right)^2 + 4} - \frac{Q_{\text{DG}}}{Q_{\text{P}_{\text{DG}}}} \right] \times \left[\sqrt{\left(\frac{Q_{\text{Load}}}{Q_{\text{P}_{\text{Load}}}}\right)^2 + 4} - \frac{Q_{\text{Load}}}{Q_{\text{P}_{\text{Load}}}} \right] \quad (16)$$

Allowable frequency variation is between f_{low} and f_{high} , the NDZ is as presented in (17).

$$Q \left(\left(\frac{f_{\text{low}\sigma}}{f} - \frac{f}{f_{\text{low}\sigma}} \right) \leq \frac{Q_{\text{Load}}}{P_{\text{DG}}} \leq Q \left(\frac{f_{\text{high}\sigma}}{f} - \frac{f}{f_{\text{high}\sigma}} \right) \right) \quad (17)$$

Where:

$$\sigma = \frac{1}{2} \left[\sqrt{\left(\frac{Q_{\text{DG}}}{Q_{\text{PDG}}} \right)^2 + 4} + \frac{Q_{\text{DG}}}{Q_{\text{PDG}}} \right]$$

Increasing the injected reactive power reduces NDZ but causes more PQ issues in return.

2.3. Active islanding detection scheme III – (Even harmonic perturbation (EHP))

In the proposed EHP method, even harmonics are intentionally introduced into q axis current. This causes ROCOF during the distributed generation's islanding state. During grid-tied operation, the grid serves as an effectively infinite sink, absorbing and neutralizing all injected disturbances. The generation of even harmonic perturbations is achieved by the application of Park and inverse Park's transformations given by (18) and (19).

$$\begin{bmatrix} \text{ud} \\ \text{uq} \\ \text{u0} \end{bmatrix} = \frac{2}{3} \begin{bmatrix} \cos\theta & \cos\left(\theta - \frac{2\pi}{3}\right) & \cos\left(\theta + \frac{2\pi}{3}\right) \\ -\sin\theta & -\sin\left(\theta - \frac{2\pi}{3}\right) & -\sin\left(\theta + \frac{2\pi}{3}\right) \\ \frac{1}{2} & \frac{1}{2} & \frac{1}{2} \end{bmatrix} \begin{bmatrix} \text{ua} \\ \text{ub} \\ \text{uc} \end{bmatrix} \quad (18)$$

$$\begin{bmatrix} \text{ua} \\ \text{ub} \\ \text{uc} \end{bmatrix} = \frac{2}{3} \begin{bmatrix} \sin\theta & \cos\theta & 1 \\ \sin\left(\theta - \frac{2\pi}{3}\right) & \cos\left(\theta - \frac{2\pi}{3}\right) & 1 \\ \sin\left(\theta + \frac{2\pi}{3}\right) & \cos\left(\theta + \frac{2\pi}{3}\right) & 1 \end{bmatrix} \begin{bmatrix} \text{ud} \\ \text{uq} \\ \text{u0} \end{bmatrix} \quad (19)$$

3. RESPONSE OF THE PASSIVE METHOD

After the perturbations are fed from the DG inverter, the response is to be monitored to identify the islanding scenario. The perturbations, used in the three active methods in this work are, injected through q axis current. Q axis current is a major deciding factor of reactive power from inverter. In the event of a mains failure, frequency change is determined by reactive power. In order to detect the islanding situation in addition to each of the current approaches, ROCOF is the preferred answer. 1 Hz/s is the threshold set for this method. Voltage THD is also measured and its upper limit is set at 5%. When both ROCOF and THD go above the threshold limits, islanding is confirmed.

3.1. ROCOF measurement

ROCOF based islanding detection works on the principle that the PCC frequency variation is manifested during the transition to an islanding state. The frequency measurement is done through a phase locked loop module. Rate of change of frequency calculated is passed through a low pass filter to filter out the noises. Then its absolute value is found out. The implementation of ROCOF is depicted in Figure 2. A trip signal is initiated if the measured value of ROCOF is greater than a threshold, which is 1 Hz/s.

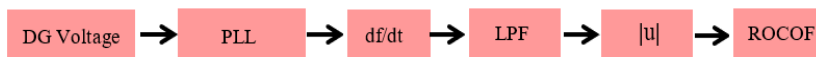


Figure 2. Block diagram of ROCOF measurement

3.2. THD measurement of DG voltage

Islanding detection methods based on harmonic distortion analysis involve the continuous monitoring of harmonic variations resulting from load changes in isolated DGs. Specifically, in DGs featuring inverter-based generation units, the operation of these inverters introduces distinct harmonic components. Detecting islanding scenarios can be accomplished through the measurement of harmonic distortions in either voltage or current signals. A viable approach for leveraging harmonic distortions in islanding detection is the computation

of total harmonic distortion (THD) and the monitoring of its fluctuations over time. The measurement of THD in DG voltage is conducted using (20), in which, V_1 represents the root mean square (RMS) value of the fundamental voltage component, while V_h signifies the RMS value of the harmonic component with index 'h.' The variable 'N' denotes the maximum number of considered harmonic components.

$$V_{\text{THD}} = 100 \sqrt{\frac{\sum_{h=2}^N V_h^2}{V_1^2}} \% \quad (20)$$

4. RESULTS AND VALIDATION

The MATLAB simulation in Simulink uses a 50 kW DG powered by solar energy and is depicted in Figure 3. The output voltage of DC/DC converter is 900 V. The DG has a local parallel RLC load and is tied with grid at PCC. The islanding is simulated at 4.2s. The simulation details are illustrated in Table 2. The variation in irradiation and bus voltage are presented in Figure 4 and Figure 5. The voltages are shown in the Figure 6. The corresponding currents are depicted in Figure 7.

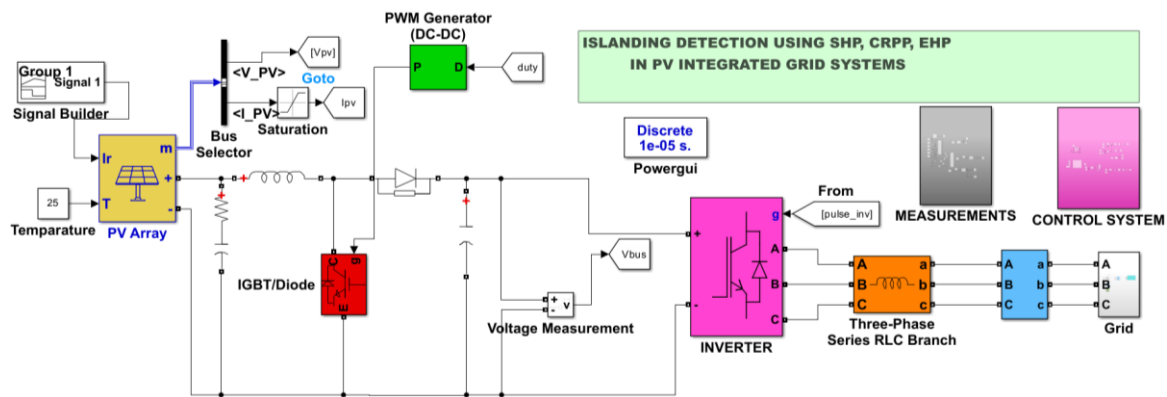


Figure 3. Simulation diagram of the IDM in grid synchronized DG

Table 2. Test system details

Features		Ratings
Load		50 kW
Q factor		2.5
f_s		5,000 Hz
V_p		245 V
DC bus Voltage		900 V
f_0		50
SHP	f_{SHP}	20 Hz
	$I_{d \text{SHP}}$	1% of id-rated
CRPP	$i_{q \text{CRPP}}$	15 A
EHP	$i_{q \text{EHP}}$	1.2 A
Load details	Resistance, R	3.4 Ω
	Inductance, L	0.00431 H
	Capacitance, C	0.0023 F

4.1. Sub harmonic perturbation (SHP)

The SHP is incorporated into the q-axis current of the inverter system. Specifically, a 20 Hz SHP of sufficient magnitude, equal to 1% of the rated I_d , is introduced into the q-axis current of the inverter as presented in Figure 8. The ROCOF during islanding is depicted in Figure 9. As soon as the loss of mains happens at 4.2s, ROCOF exceeds the threshold of 1Hz/sec, at $t = 4.42s$. Thereby islanding state is confirmed. The THD has gone above the threshold of 5%. THD of DG voltage during grid synchronized as well as islanding state are shown in the Figure 10(a) and Figure 10(b). The SHI induces low-frequency oscillations in the DG absolute frequency, when it operates in an islanded state. Notably, these oscillations are absent in grid connected distributed generation (GCDG) mode, as sub-harmonics are efficiently channeled directly into the utility grid. But in the islanded mode these oscillations are present. This observation is illustrated in Figure 11(a) and Figure 11(b).

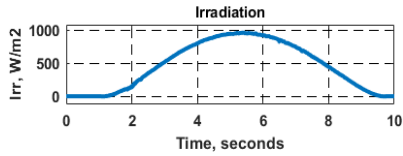


Figure 4. Variation of irradiation

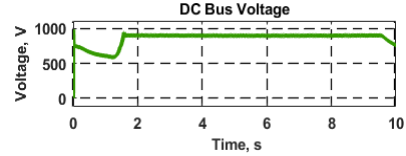


Figure 5. DC link voltage

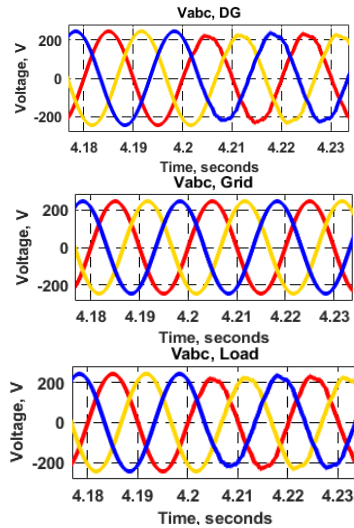


Figure 6. DG-voltage, grid voltage, and load voltage

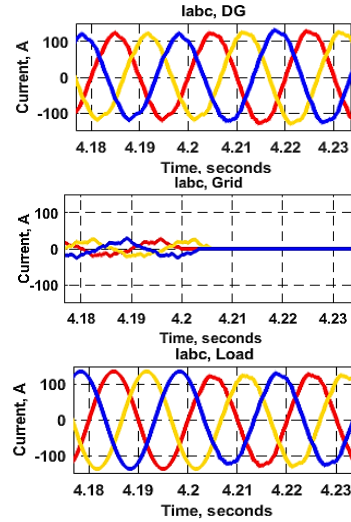


Figure 7. DG current, grid current, and load current

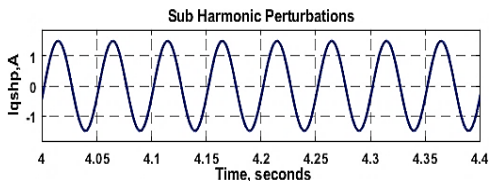


Figure 8. SHP injected from DG inverter

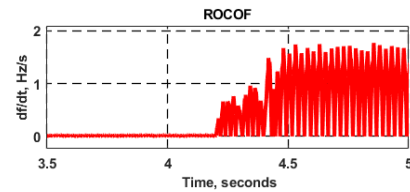
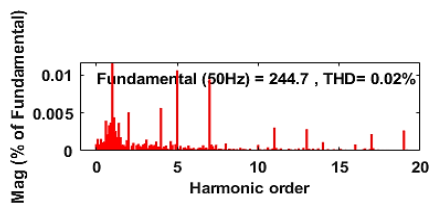
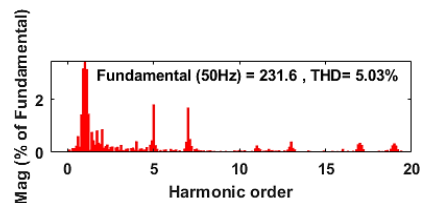


Figure 9. ROCOF in SHP method

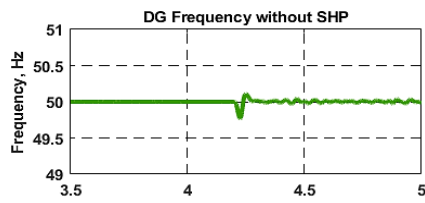


(a)

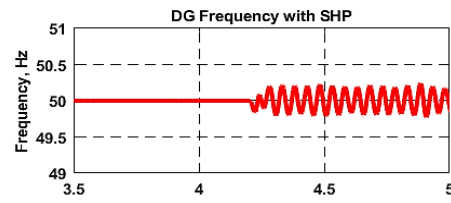


(b)

Figure 10. THD of DG voltage in SHP during (a) grid synchronized mode and (b) during islanding mode



(a)



(b)

Figure 11. Oscillations in the frequency waveform during islanding state (a) with SHP (b) without SHP

4.2. Complementary reactive power perturbation (CRPP)

In the Figure 12, CRPP injected from the DG inverter is presented. The ROCOF is shown in Figure 13. The THD has beyond the 5% cutoff point as soon as the loss of mains happens at 4.2 seconds. ROCOF exceeds the threshold of 1Hz/s at t=4.3 seconds after the occurrence of islanding at 4.2 s. The THDs of DG voltage during grid synchronized as well as islanding state are shown in the Figures 14(a) and 14(b).

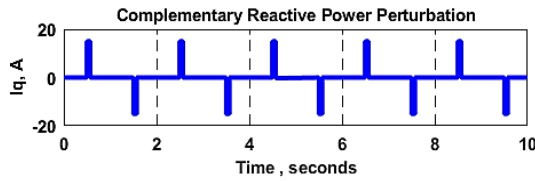


Figure 12. Complementary reactive power perturbation

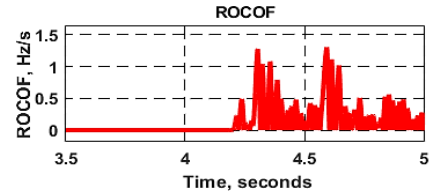


Figure 13. The ROCOF in CRPP method

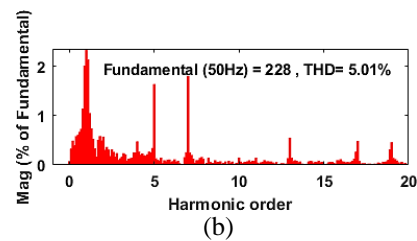
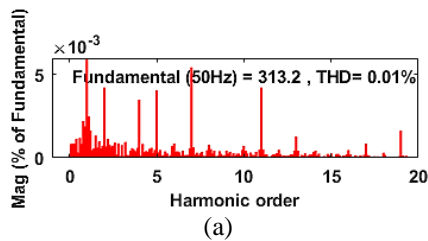


Figure 14. THD of DG voltage in CRPP during (a) grid synchronized mode, and (b) islanding mode

4.3. Even harmonic perturbation (EHP)

Even harmonics injected along with the q axis current is depicted in Figure 15. The injection of even harmonics causes the ROCOF to go beyond the threshold of 1Hz/s at t=4.57seconds after the occurrence of islanding at 4.2 s, which is shown in Figure 16. THDs of DG voltage during grid synchronized as well as islanding state are shown in the Figures 17(a) and 17(b).

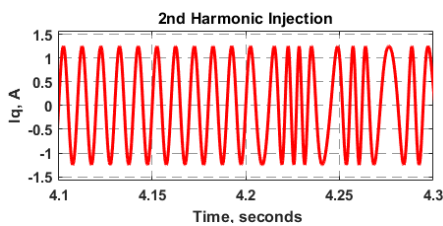


Figure 15. Injected second order harmonics

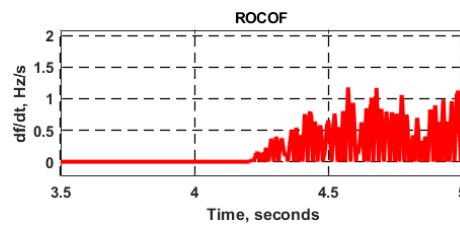


Figure 16. The ROCOF in EHP method

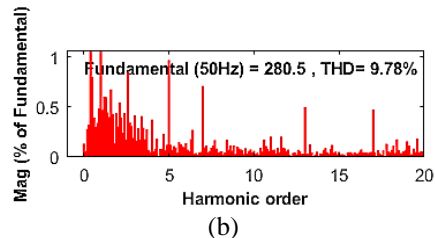
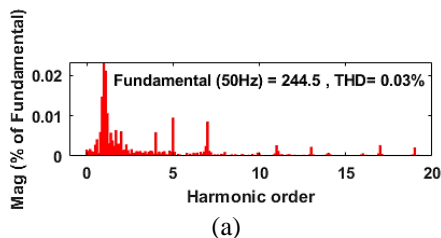


Figure 17. THD of DG voltage in EHP during (a) grid synchronized mode and (b) islanding mode

5. COMPARISON OF SHP, CRPP AND EHP

The comparative analysis of NDZ and FDZ of the three approaches are presented in Table 3. The THD values of DG voltage during grid synchronized mode for different load quality factors is presented in Table 4. It is also shown in Figure 18. CRPP method shows least THD during grid synchronized mode. The THD values of DG voltage during islanded mode for different load quality factors is presented in Table 5. It is also shown in Figure 19. CRPP method shows least THD during grid synchronized mode. The islanding detection time of three methods for various load quality factors are presented in Table 6 and is also shown in Figure 20. CRPP method shows least THD during both islanding mode and Grid Integrated mode. The detection time of the three approaches (SHP, CRPP, EHP) are compared with the existing methods and is presented in Figure 21. CRPP approach has the least detection time as it is closest to the center of the radar web.

Table 3. Comparison of NDZ and FDZ

Method	NDZ		FDZ			
	$\Delta P=0, \Delta Q=0$	Load QF	3 phase Induction Motor Load switching (20hp)	3 phase capacitor bank switching(25kVAR)	3-Phase and LLG faults ($Z_f = 0.01\Omega$)	Non-Linear Load (Bridge Rectifier with 25kW Load)
SHP	As $\Delta P < 5\%$ Detection time goes above 2s	No NDZ up to QF=5	No False tripping	No False tripping	No False tripping	No False tripping
CRPP	No NDZ	No NDZ up to QF=5	No False tripping	No False tripping	No False tripping	No False tripping
EHP	No NDZ	No NDZ up to QF=5	No False tripping	No False tripping	No False tripping	No False tripping

Table 4. THD of DG voltage in GC mode

QF=1	QF=1.5	QF=2	QF=2.5	QF=3	QF=4	QF=5
0.1	0.08	0.05	0.03	0.02	0.01	0.009
0.07	0.05	0.04	0.02	0.015	0.01	0.009
0.07	0.04	0.03	0.01	0.01	0.009	0.008

Table 5. THD % in Islanded mode

IDMs	QF=0.5	QF=1	QF=1.5	QF=2	QF=2.5	QF=3	QF=4	QF=5
EHP	12	11.2	10.9	9.9	9.78	9.3	9	8.5
SHP	7.2	6.5	5.8	5.2	5.03	4.9	4.7	4.55
CRPP	7	6.2	5.5	5.1	5.01	4.8	4.1	3.9

Table 6. Islanding detection time (IDT)

IDMs	QF=0.5	QF=1	QF=1.5	QF=2	QF=2.5	QF=3	QF=4	QF=5
EHP & ROCOF	0.31	0.32	0.33	0.35	0.37	0.39	0.4	0.42
SHP & ROCOF	0.15	0.16	0.18	0.2	0.22	0.24	0.25	0.27
CRPP & ROCOF	0.082	0.086	0.09	0.095	0.1	0.13	0.14	0.16

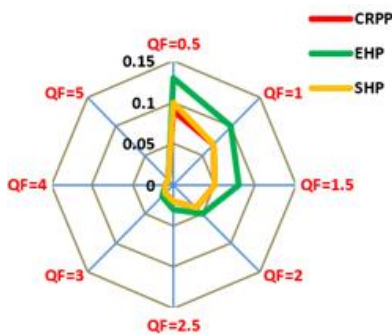


Figure 18. THD% in grid synchronized mode

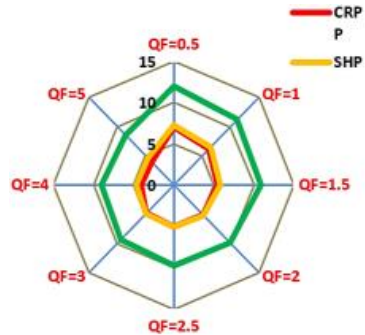


Figure 19. THD% in islanded mode

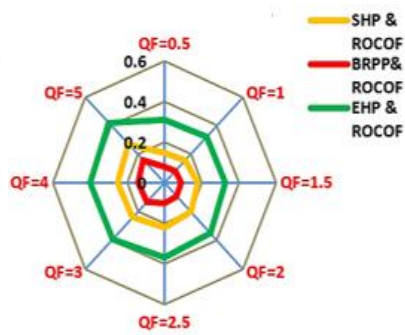


Figure 20. Islanding detection time for different load quality factors

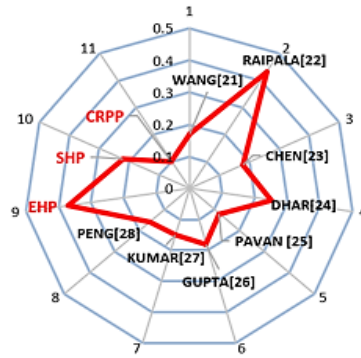


Figure 21. Comparison of Islanding detection time of the three approaches with the existing methods

6. CONCLUSION

The performance assessment of three q axis perturbation based active islanding detection methods (SHP, CRPP, EHP) are presented in this paper. The NDZ and FDZ analysis are also presented in this paper. In all three approaches, ROCOF has exceeded the 1Hz/sec threshold limit when an islanding condition occurs. From the results it has been identified that the CRPP method is able to detect the islanding scenario with least detection time of 0.1seconds (QF=2.5). THD of DG voltage is least for CRPP method during grid synchronized mode. But this superior method is able to drift the %THD of DG voltage well beyond the threshold value of 5%, which is a desirable feature of any active method. Therefore, the CRPP method outperforms the SHI and EHP methods for various load quality factors.




REFERENCES

- [1] N. K. Kasim, N. M. Obaid, H. G. Abood, R. A. Mahdi, and A. M. Humada, "Experimental study for the effect of dust cleaning on the performance of grid-tied photovoltaic solar systems," *International Journal of Electrical and Computer Engineering*, vol. 11, no. 1, pp. 74–83, 2021, doi: 10.11591/ijece.v11i1.pp74-83.
- [2] T. Ikra Rahman, A. Fariha Rashid, and M. H. Rahman, "Design and development of Bi directional power meter using microcontroller," *Indonesian Journal of Electrical Engineering and Computer Science*, vol. 17, no. 3, p. 1594, Mar. 2020, doi: 10.11591/ijeecs.v17.i3.pp1594-1600.
- [3] J. Kumar, N. R. Parhyar, M. K. Panjwani, and D. Khan, "Design and performance analysis of PV grid-tied system with energy storage system," *International Journal of Electrical and Computer Engineering (IJECE)*, vol. 11, no. 2, p. 1077, Apr. 2021, doi: 10.11591/ijece.v11i2.pp1077-1085.
- [4] A. A. Adebisi, I. J. Lazarus, A. K. Saha, and E. E. Ojo, "Performance analysis of grid-tied photovoltaic system under varying weather condition and load," *International Journal of Electrical and Computer Engineering (IJECE)*, vol. 11, no. 1, p. 94, Feb. 2021, doi: 10.11591/ijece.v11i1.pp94-106.
- [5] "IEEE Standard for Interconnection and Interoperability of Distributed Energy Resources with Associated Electric Power Systems Interfaces--Amendment 1: To Provide More Flexibility for Adoption of Abnormal Operating Performance Category III," *IEEE Std 1547a-2020 (Amendment to IEEE Std 1547-2018)*, pp. 1–16, 2020, doi: 10.1109/IEEESTD.2020.9069495.
- [6] J. C. M. Vieira, D. Salles, and W. Freitas, "Power imbalance application region method for distributed synchronous generator anti-islanding protection design and evaluation," *Electric Power Systems Research*, vol. 81, no. 10, pp. 1952–1960, 2011, doi: 10.1016/j.epsr.2011.06.009.
- [7] D. Velasco, C. L. Trujillo, G. Garcerá, and E. Figueres, "Review of anti-islanding techniques in distributed generators," *Renewable and Sustainable Energy Reviews*, vol. 14, no. 6, pp. 1608–1614, 2010, doi: 10.1016/j.rser.2010.02.011.
- [8] R. A. Walling, "Application of direct transfer trip for prevention of DG islanding," *IEEE Power and Energy Society General Meeting*, 2011, doi: 10.1109/PES.2011.6039727.
- [9] D. Motter and J. C. M. Vieira, "Improving the islanding detection performance of passive protection by using the undervoltage block function," *Electric Power Systems Research*, vol. 184, 2020, doi: 10.1016/j.epsr.2020.106293.
- [10] N. Ikken, N. E. Tariba, A. Bouknadel, A. Haddou, H. El Omari, and H. El Omari, "A fuzzy rule based approach for islanding detection in grid connected inverter systems," *International Journal of Electrical and Computer Engineering*, vol. 11, no. 6, pp. 4759–4766, 2021, doi: 10.11591/ijece.v11i6.pp4759-4766.
- [11] R. Chandrakar, R. K. Dubey, and B. K. Panigrahi, "THD-Based Passive Islanding Detection Technique for Droop-Controlled Grid-Forming Inverters," *IEEE Systems Journal*, 2023, doi: 10.1109/JSYST.2023.3283265.
- [12] S. Nikolovski, H. R. Baghaee, and D. Mlatic, "Islanding Detection of Synchronous Generator-Based DGs using Rate of Change of Reactive Power," *IEEE Systems Journal*, vol. 13, no. 4, pp. 4344–4354, 2019, doi: 10.1109/JSYST.2018.2889981.
- [13] J. Merino, P. Mendoza-Araya, G. Venkataramanan, and M. Baysal, "Islanding Detection in Microgrids Using Harmonic Signatures," *IEEE Transactions on Power Delivery*, vol. 30, no. 5, pp. 2102–2109, 2015, doi: 10.1109/TPWRD.2014.2383412.
- [14] D. Reigosa, F. Briz, C. B. Charro, P. Garcia, and J. M. Guerrero, "Active islanding detection using high-frequency signal injection," *IEEE Transactions on Industry Applications*, vol. 48, no. 5, pp. 1588–1597, 2012, doi: 10.1109/TIA.2012.2209190.
- [15] S. Murugesan, V. Murali, and S. A. Daniel, "Hybrid Analyzing Technique for Active Islanding Detection Based on d-Axis Current Injection," *IEEE Systems Journal*, vol. 12, no. 4, pp. 3608–3617, 2018, doi: 10.1109/JSYST.2017.2730364.
- [16] Y. Elshrief, A. Dania, S. Abd-Elhaleem, and B. A. Zalam, "On active anti-islanding techniques: survey," *Indonesian Journal of Electrical Engineering and Computer Science*, vol. 22, no. 2, pp. 609–618, 2021, doi: 10.11591/ijeecs.v22.i2.pp609-618.




- [17] N. A. Gajjar, T. Zaveri, and N. Zaveri, "Adaptive I0-LMS based algorithm for solution of power quality problems in PV-STATCOM based system," *Bulletin of Electrical Engineering and Informatics*, vol. 12, no. 2, pp. 608–618, 2023, doi: 10.11591/eei.v12i2.4174.
- [18] V. Nougain, S. Prakash, and S. Mishra, "Hybrid Islanding Detection Method based on ROCOF over Reactive Power and d-Axis Current Injection," *India International Conference on Power Electronics, IICPE*, vol. 2018-Decem, 2018, doi: 10.1109/IICPE.2018.8709518.
- [19] M. Seyedi, S. A. Taher, B. Ganji, and J. Guerrero, "A Hybrid Islanding Detection Method Based on the Rates of Changes in Voltage and Active Power for the Multi-Inverter Systems," *IEEE Transactions on Smart Grid*, vol. 12, no. 4, pp. 2800–2811, 2021, doi: 10.1109/TSG.2021.3061567.
- [20] M. Khodaparastan, H. Vahedi, F. Khazaeli, and H. Oraee, "A Novel Hybrid Islanding Detection Method for Inverter-Based DGs Using SFS and ROCOF," *IEEE Transactions on Power Delivery*, vol. 32, no. 5, pp. 2162–2170, 2017, doi: 10.1109/TPWRD.2015.2406577.
- [21] G. Wang, F. Gao, J. Liu, Q. Li, and Y. Zhao, "Design consideration and performance analysis of a hybrid islanding detection method combining voltage unbalance/total harmonic distortion and bilateral reactive power variation," *CPSS Transactions on Power Electronics and Applications*, vol. 5, no. 1, pp. 86–100, 2020, doi: 10.24295/CPSS TPEA.2020.00008.
- [22] O. Raipala, A. S. Makinen, S. Repo, and P. Jarventausta, "An Anti-Islanding Protection Method Based on Reactive Power Injection and ROCOF," *IEEE Transactions on Power Delivery*, vol. 32, no. 1, pp. 401–410, 2017, doi: 10.1109/TPWRD.2016.2543503.
- [23] X. Chen, Y. Li, and P. Crossley, "A novel hybrid islanding detection method for grid-connected microgrids with multiple inverter-based distributed generators based on adaptive reactive power disturbance and passive criteria," *IEEE Transactions on Power Electronics*, vol. 34, no. 9, pp. 9342–9356, 2019, doi: 10.1109/TPEL.2018.2886930.
- [24] S. Dhar and P. K. Dash, "Harmonic profile injection-based hybrid active islanding detection technique for PV-VSC-based microgrid system," *IEEE Transactions on Sustainable Energy*, vol. 7, no. 4, pp. 1473–1481, 2016, doi: 10.1109/TSTE.2016.2515158.
- [25] Y. Pavankumar, S. Debnath, and S. Paul, "A New Lissajous-Based Technique for Islanding Detection in Microgrid," *IEEE Transactions on Smart Grid*, 2023, doi: 10.1109/TSG.2023.3322435.
- [26] P. Gupta, R. S. Bhatia, and D. K. Jain, "Average absolute frequency deviation value based active islanding detection technique," *IEEE Transactions on Smart Grid*, vol. 6, no. 1, pp. 26–35, 2015, doi: 10.1109/TSG.2014.2337751.
- [27] A. Kumar, A. Mohapatra, and S. N. Singh, "Phaselet-Based Limited-Time q-Axis DC Offset Voltage Injection for Detection of Islanding of DG and Fault in a Meshed Microgrid," *IEEE Systems Journal*, vol. 16, no. 1, pp. 1379–1390, 2022, doi: 10.1109/JSYST.2021.3068397.
- [28] T. Peng, C. Bai, X. Song, and S. Duan, "An Islanding Detection Method Based on the Reactive Power Disturbance for Multiple Inverter-Based DG Systems," *IEEE Transactions on Industrial Electronics*, vol. 71, no. 4, pp. 3253–3263, 2024, doi: 10.1109/TIE.2023.3274875.

BIOGRAPHIES OF AUTHORS



Praveen Raj Rajaswamy Sarojam    received his B.E. degree in electrical and electronics engineering from CSI Institute of Technology, Thovalai, Tamil Nadu, MS University in 2002 and M.Tech. degree in electrical engineering from College of Engineering Trivandrum, Kerala University in 2009. His research interests include smart grids, micro grids, islanding and electric vehicle charging systems. He can be contacted at email: praveenraj.rs@mbcet.ac.in.



Joseph Sarojini Savier    received his M.E. degree in electrical engineering from IISc Bangalore and Ph.D. degree in electrical engineering from IIT Kharagpur. Currently, he is working as Principal at College of Engineering Trivandrum, Kerala. His research interests include smart grids, micro-grids, distribution systems, power system protection and energy storage. He can be contacted at email: savierjs@yahoo.com.